Contents list available at CBIORE journal website

International Journal of Renewable Energy Development

Journal homepage: https://ijred.cbiore.id

Research Article

# Performance of sulfided NiMo catalyst supported on pillared bentonite Al and Ti under hydrodeoxygenation reaction of guaiacol

Nino Rinaldi[a*], Novi Liana Sari[a,b], Sumari[b], Anis Kristiani[a], Egi Agustian[a], Robert Ronald Widjaya[a], Adid Adep Dwiatmoko[a]

[a]*Research Center for Chemistry, National Research and Innovation Agency, Indonesia*

[b]*Department of Chemistry, Faculty of Mathematics and Natural Sains, Malang State University, Indonesia*

**Abstract**. Bio-crude oil is known to be sustainable, eco-environmentally, and an alternative energy source produced by biomass pyrolysis. However, its quality remains relatively low due to a higher oxygen concentration compared to liquid fuels from fossils. Therefore, an upgrading process is necessary through the catalytic hydrodeoxygenation (HDO) process. This work synthesized pillared bentonite using Al and Ti metals as the pillaring agent to produce Al-PILC and Ti-PILC as catalyst support for sulfided NiMo. Their catalytic activity in HDO reaction using guaiacol as a model compound of bio-crude oil were also evaluated. Characterization of the bentonite-pillared materials, including Al-PILC, Mo/Al-PILC, NiMo/Al-PILC, Ti-PILC, Mo/Ti-PILC, and NiMo/Ti-PILC, was performed using Surface Area Analyzer, X-ray Diffractometer (XRD), Temperature-Programmed Desorption of ammonia ($NH_3$-TPD), X-Ray Fluorescence (XRF), and Scanning Electron Microscope (SEM) techniques. The characterization results confirm the pillarization process of bentonite using Al and Ti metals as the pillaring agent, and the preparation of the NiMo catalyst using the stepwise impregnation method was successfully prepared. The NiMo/Ti-PILC catalyst performs a superior conversion value on the HDO guaiacol reaction than other catalysts. A well dispersion of Mo and Ni metals on the surface support (NiMo/Ti-PILC), thus creating numerous active sites of the catalyst after the sulfidation. Variations in time and temperature during the HDO guaiacol reaction significantly affected the conversion.

**Keywords:** bentonite, pillarization, Ni-Mo catalyst, hydrodeoxygenation, guaiacol



Received: 8th January 2023; Revised: 28th March 2024; Accepted: 16th April 2024; Available online: 24th April 2024

## 1. Introduction

Nowadays, the depletion of fossil fuels and increasing energy needs are important reasons for developing alternative energy sources. One alternative energy source with enormous potential is biomass (Annisa, 2012). The most commonly used method for converting biomass into liquid fuel is pyrolysis, which falls under Thermo-Chemical Conversion. This process is more efficient than biochemical processes due to its ability to decompose bio-polymer compounds such as lignin (Adams *et al.*, 2018). Bio-crude oil results from biomass pyrolysis that can be used as an environmentally friendly and sustainable alternative to fuel oil (Mohan *et al.*, 2006; Mortensen *et al.*, 2011). However, bio-crude oil as an energy source, especially fuel, still faces defiance due to its high oxygen content. The increased oxygen content leads to low calorific value, high viscosity, chemical instability, and high acidity (Liu, 2016). Therefore, additional processes are required to improve bio-crude oil quality, one of which is the hydrodeoxygenation process.

Hydrodeoxygenation (HDO) is a reaction aimed at eliminating oxygen atoms and breaking double bonds through hydrogen gas (de Miguel Mercader *et al.*, 2011). Bio-crude oil major consists of polyaromatic hydrocarbon compounds containing various aldehydes, alcohols, furfural, ketones, carboxylic acids, anisole, guaiacol, and more. Therefore, understanding the HDO reaction for bio-crude oil can be remarkably challenging and therefore researchers have employed bio-crude oil model compounds to get deeper information into this study. Model compounds offer several advantages, including providing precise chemical mechanism information, preventing thermal polymerization, and elucidating product selectivity (Liu, 2016). Guaiacol was selected as a model compound for studying the HDO process due to its presence in bio-crude oil derived from lignin, a common component of bio-crude oil pyrolysis (Nugrahaningtyas *et al.*, 2015). The HDO reaction of guaiacol yields compounds such as phenol, toluene, benzene, cyclohexane, catechol, and more.

Using a catalyst in the Hydrodeoxygenation (HDO) reaction plays a crucial role. Previous research showed that several active metals were used on the HDO catalysts, such as sulfided active metals (NiMoS), noble metals (Ru, Rh, Pd, and Pt), and base metals (Fe, Ni, and Cu). (Bu *et al.*, 2012), Using metal sulfide and base metal catalysts in HDO reactions often results in comparable or even superior product yields compared to noble metal catalysts (Kubička & Kaluža, 2010; Lee *et al.*, 2012; Mora-Vergara *et al.*, 2018). The NiMoS catalyst, in its active phase, exhibits a low surface area, which hinders effective and

* Corresponding author
Email: nino002@brin.go.id (N. Rinaldi)

https://doi.org/10.61435/ijred.2024.60060
ISSN: 2252-4940/© 2024.The Author(s). Published by CBIORE

efficient interaction between the reactants and the active centers. Therefore, it is necessary to disperse the active metals Ni and Mo onto the support surface (Kabe, T., Ishihara, A., Qian, 1999; Topsøe, H.; Clausen, B.S.; Massoth, 1996). The addition of sulfur into NiMo aims to activate the catalyst, increase the acidity, and facilitate the HDO reaction of guaiacol (Mora-Vergara *et al.*, 2018).

Alumina oxide ($Al_2O_3$) is commonly used to support industrial-scale bio-crude oil HDO reactions (Mora-Vergara *et al.*, 2018). However, one drawback is that catalyst deactivation can occur during the HDO reaction due to the formation of phenate sourced from alumina as catalyst support (Şenol *et al.*, 2005). Thus, the choice of catalyst support is an important step. One of the potential support materials is natural materials like bentonite clay minerals. Bentonite is found all over the world and is environmentally friendly. It is well-known as low-cost catalyst support (Amaya *et al.*, 2020; Kar, 2018). Due to cost-efficiency, the use of bentonite clay minerals is more favorable compared to expensive synthetic catalysts. Bentonite has several unique properties, such as a high swelling ability and cation exchange capacity (Amaya *et al.*, 2020). However, its utilization still needs to be improved. One method to enhance the utility of bentonite and make it economically valuable is the Pillared Inter-Layer Clay (PILC) treatment. Pillarization is an intercalation process of pillaring agents generally using metals with specific sizes and charges, such as Al, Mn, Ti, and other metal oxides (Binitha & Sugunan, 2006; Haerudin *et al.*, 2010; Salerno *et al.*, 2004; Sumarlan *et al.*, 2017; Widjaya, 2012). Depending on the reaction type, it can be ion exchanged between layered bentonite materials. The primary goal of pillarization is to modify bentonite's physical and chemical properties, including increasing its surface area, porosity, and thermal stability. Several metal oxides such as Al, Zr, Ti, Fe, and Cr have been successfully used as pillar agents in the bentonite pillarization process and create different physicochemical properties from each other reported in our previous works (Khairina *et al.*, 2022; Rinaldi *et al.*, 2023, 2017). Bentonite pillarization using Ti resulted in the increase in specific surface area from 24.47 $m^2/g$ to more than 150 $m^2/g$ and acidity from 0.08 mmol/g to 0.66 mmol/g due to the bond between metals and the alumina-silicate bentonite layer (Khairina *et al.*, 2022). According to Salerno in Adilina *et al* (2019), the NiMoS catalyst supported by bentonite shows better activity in the HDO reaction than that supported by alumina (Adilina *et al.*, 2019).

Therefore, this work synthesized pillared bentonite using Al and Ti metals as the pillaring agents to produce Al-PILC and Ti-PILC as catalyst support for sulfided NiMo. Their catalytic activity in the HDO reaction using guaiacol as a model compound of bio-crude oil was also investigated. Several sophisticated characterizations were conducted to obtain their physicochemical properties. To our knowledge, there are still no reports in the literature about sulfided NiMo catalysts supported on pillared bentonite Al and Ti for the hydrodeoxygenation reaction of guaiacol.

## 2. Materials and Methods

### *2.1 Materials*

Guaiacol was used as a bio-crude oil model compound. Guaiacol and bentonite were purchased from Sigma-Aldrich and used without further purification. Nickel nitrate hexahydrate ($Ni(NO_3)_2.6H_2O$), ammonium heptamolybdate tetrahydrate ($(NH_4)_6Mo_7O_{24}{\cdot}4H_2O$), aluminum chloride ($AlCl_3$), sodium hydroxide (NaOH), titanium (IV) isopropoxide ($Ti(OCH(CH_3)_2)_4$), benzene, cyclohexane, phenol, and decan were obtained from Merck in p.a grade.

### *2.2 Synthesis of NiMo/Al-PILC and NiMo/Ti-PILC*

PILC was prepared by synthesizing a polycation solution. The Al polycation solution was prepared by slowly dissolving aluminum chloride (13.35 g, 10 mmol/g-clay) in 1000 mL distilled water and stirring for 2 hours at room temperature. The sodium hydroxide solution (8 g in 1000 mL distilled water, ratio mole $OH^-/Al^{3+}$ = 2) was then added to the Al polycation solution using a peristaltic pump and stirred for 12 hours (Rinaldi *et al.*, 2023; Sumarlan *et al.*, 2017). The Ti polycation solution was prepared by slowly adding 50 mL of titanium (IV) isopropoxide solution (50 mmol/g-clay) to 40 mL of 5 M HCl and homogenizing it with a magnetic stirrer for 2 hours (Binitha & Sugunan, 2006; Parangi & Mishra, 2020; Rinaldi *et al.*, 2023). Before pillarization, 10 g bentonite was swelled in 1000 mL of distilled water and stored at 333 K for 2 hours while stirring. The prepared Al and Ti polycation solution was added to the bentonite suspension for 24 hours for pillarization. The precipitate was washed using hot distilled water (333 K) until it was free of chloride ions when tested with 0.001M $AgNO_3$ reagent. The resulting PILC was filtered, dried overnight at 378 K, and calcined at 723 K for 4 hours, called Al-PILC and Ti-PILC. NiMo/Al-PILC and NiMo/Ti-PILC catalysts were prepared using a double impregnation method (Kubička & Kaluža, 2010; Mora-Vergara *et al.*, 2018; Salerno *et al.*, 2004; Xu *et al.*, 2010). The first impregnation was carried out by adding 13 wt% $MoO_3$ from ammonium heptamolybdate solution (1.28 g, 50 mL distilled water) to the Al-PILC and Ti-PILC suspension (7 g, 20 mL distilled water) to produce Mo/Al-PILC and Mo/Ti-PILC. The second impregnation was carried out by adding 4 wt% NiO from nickel nitrate hexahydrate solution (0.97 g, 20 mL distilled water) to the suspension of Mo/Al-PILC and Mo/Ti-PILC (6 g, 40 mL distilled water). In each impregnation process, the catalyst was dried at 378 K overnight and calcined at 723 K for 5 hours.

### *2.3 Catalytic HDO of Guaiacol*

The catalysts were sulfided before being utilized in the Hydrodeoxygenation (HDO) reaction. Sulfidation of the catalyst was carried out by weighing 3 % of the weight of guaiacol (0.03 g) and placing it into a glass U-shaped sulfidation tube, which was then attached to a sulfidation apparatus. In the first stage, the catalyst was purged with $N_2$ gas at a pressure of atm and a temperature of 423 K for 90 minutes. Subsequently, $H_2$ gas at atm pressure was introduced into a $CS_2$ solution, producing $H_2S$ gas. The generated $H_2S$ gas was fed into the catalyst at a temperature of 623 K for 90 minutes (Adilina *et al.*, 2019; Rinaldi *et al.*, 2017). The sulfided catalyst was used for the Hydrodeoxygenation (HDO) reaction of guaiacol. In a typical process, the sulfided catalyst (3 wt% guaiacol) was inserted into the autoclave reactor with 1 mL guaiacol and 9 mL decane solvent. The reaction was carried out at temperatures of 523 K, 573 K, and 623 K for 2, 3, and 4 hours at a constant pressure of 60 bar. The liquid product was filtered with filter paper. The guaiacol HDO product was then analyzed by GC-FID instruments, Agilent 7890A with Carbowax column/20M (30 m × 320 $\mu$m × 0,25 $\mu$m. The analysis using GC-FID aimed for quantitative analysis to calculate the percent conversion and yield of the HDO reaction.

### *2.4 Catalyst Characterization*

The Brunauer – Emmett – Teller (BET) adsorption method obtained the surface area of the pillared bentonite, which was

conducted using a Tristar II 3020 Micromeritic Instrument via a nitrogen adsorption-desorption isotherm. The degassing process used $N_2$ gas at 473 K for 2 hours. Catalyst diffraction pattern analysis was carried out using an X-ray diffractometer (XRD) apparatus, with Cu-Kα radiation (1.542 Å) and a 2θ angle range from 10° to 80° (wide angle) and a range of 2° to 10° (low angle). Pillared bentonite catalyzed total surface acidification was carried out by ChemiSorb 2750 (Micromeritics, USA) and using temperature-programmed ammonia desorption ($NH_3$-TPD). Samples were degassed in a stream of pure helium at 673 K for one hour before ammonia absorption. The sample was then saturated in a stream of $NH_3$ gas (5% in helium gas, v/v) for 30 minutes. The sample was then cleaned with a stream of helium for 15 minutes at room temperature to remove the physically absorbed $NH_3$ gas. Desorption was carried out in a pure helium flow with a linear heating rate (283 K/min) until the temperature reached 773 K. Finally, cooling was carried out to a temperature of 373 K, and obtained TCD (Thermal Conductivity Detector) signal data.

Scanning electron microscopy (SEM) was carried out to obtain information on the surface morphology of the pillared bentonite samples placed and attached to the SEM specimen holder using a carbon double type with the cross-section pointing vertically upwards. X-ray fluorescence (XRF) determined the oxide composition of bentonite and pillared bentonite samples. The sample was placed in a polyethylene container with a mylar plastic backing and then pressed until the surface was flat, and then the sample was placed in the sample holder.

## 3. Results and Discussion

### *3.1 Characterization results*

The characterization was conducted to determine whether the pillarization or the impregnation process of the prepared NiMo/Al-PILC and NiMo/Ti-PILC catalysts have been carried out successfully. Catalyst characterization using the BET method is based on the nitrogen ($N_2$) gas adsorption and desorption process to evaluate the prepared catalysts' surface area, pore volume, and average pore size. Table 1 shows the results of nitrogen gas adsorption characterization.

It reveals in Table 1 a significant increase in bentonite's surface area ($S_{BET}$) after it was pillared with aluminum and titanium polycations. This increase is caused by the formation of hydrolysis of $Al^{3+}$ ions, leading to the formation of large Al cation polymers known as kegging ions $[Al_{13}O_4(OH)_{24}(H_2O)_{12}]^{7+}$, which have a relatively uniform size of pore diameter (Smart *et al.*, 2005). Similarly, $Ti^{4+}$ ions form polycations $[(Ti_8O_8(OH)_{12}]^{4+}$. However, there is a decrease in $S_{BET}$ following the impregnation of Mo and Ni met. The decline occurs because some of the Ni and Mo metals occupy the surface and into the pores of bentonite, thereby covering the pores and reducing the surface area and the pore volume (Adilina *et al.*, 2019).

**Table 1**
The $N_2$ gas adsorption results using BET method.

| Samples | Surface Area ($m^2/g$) | Pore volume ($cm^3/g$) | *Pore diameter (nm) |
|---|---|---|---|
| Bentonit | 30.26 | 0.08 | 14.25 |
| Al-PILC | 169.10 | 0.16 | 9.87 |
| Mo/Al-PILC | 102.77 | 0.12 | 12.81 |
| NiMo/Al-PILC | 83.25 | 0.09 | 11.15 |
| Ti-PILC | 187.89 | 0.22 | 4.59 |
| Mo/Ti-PILC | 149.52 | 0.19 | 5.19 |
| NiMo/Ti-PILC | 130.45 | 0.17 | 5.36 |

* is determined by the highest point of P-P0 (adsorption-desorption)

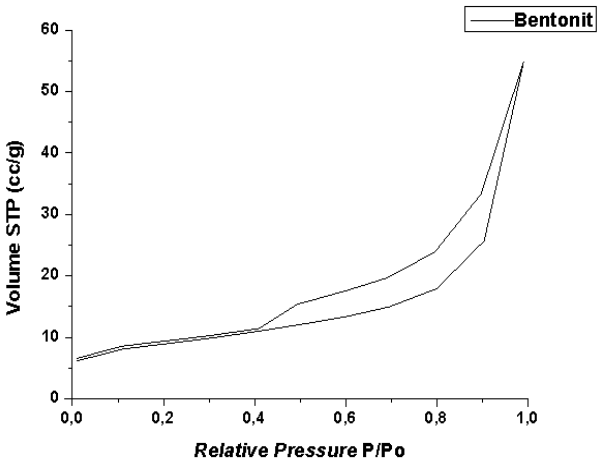


**Fig 1.** Bentonite's Adsorption-Desorption isotherm graph.

Table 1 also observes a slight increase of the pore size after the impregnation, suggesting some Ni and Mo metals also interacted and contributed as the pillared between bentonite layers. However, Ni and Mo metals mostly dispersed on the surface and pores of bentonite. According to Lui (2016), during the impregnation process, metals can be distributed both on the surface and within the pores of the catalyst, leading to changes in the measured parameters (Liu, 2016). The types of pores generated can be observed in Figure 1, representing the adsorption-desorption isotherm graph of bentonite.

The hysteresis loop type exhibited by the bentonite is of type H3 (Fig. 1). This conforms with Thommes' statement (2015) that clay (bentonite) commonly forms the H3-type loops. Moreover, Fig. 1 also describes that bentonite is categorized as a type IV isotherm with a mesoporous pore type (Thommes *et al.*, 2015). Table 1 shows that the pore size of bentonite is around 14.25 nm, which is classified as a mesoporous type(Sing, 1982). Figure 2 shows the adsorption-desorption isotherm graph of the prepared catalyst. Based on Figure 2, the type of pores generated is mesopores. According to Thommes (2015), mesopores are characterized by the formation of cone and cylinder-shaped loops that taper at their ends, with the isotherm type being type IV (Thommes *et al.*, 2015). The appearance of mesoporous structures leads to an increase in the surface area of bentonite after the pillarization.

X-ray diffraction (XRD) is measured to determine the structure and phases formed within the material (Niemantsverdriet, 2007). Additionally, it is utilized to assess the success of the catalyst preparation process using the pillarization and stepwise wet impregnation methods, primarily to determine the basal space distance between the interlayer of bentonite in Miller indices ($d_{001}$) at the 2θ range of 2° to10°. The results of the XRD analysis for the Al/PILC and Ti/PILC samples in Figure 2 were magnified five times; this aims to ensure that the diffraction peaks can be measured more clearly. The result shows that bentonite has a diffraction peak at 2θ = 6.5° with a Miller index ($d_{001}$). After the pillarization with Al and Ti polycations, the diffraction peak $d_{001}$ shifted to 5° (Al-PILC) and 3.5° (Ti-PILC), respectively. The shift in the diffraction d001of bentonite caused an increase in basal spacing from 13.6 Å to 17.7 Å for Al-PILC and 25.2 Å for Ti-PILC, indicating the pillarization process was carried out, as supported by an increase in surface area and pore volume (Table 1). It is proposed that cation exchange has occurred in the bentonite interlayer layer with Al or Ti polycations and generates an

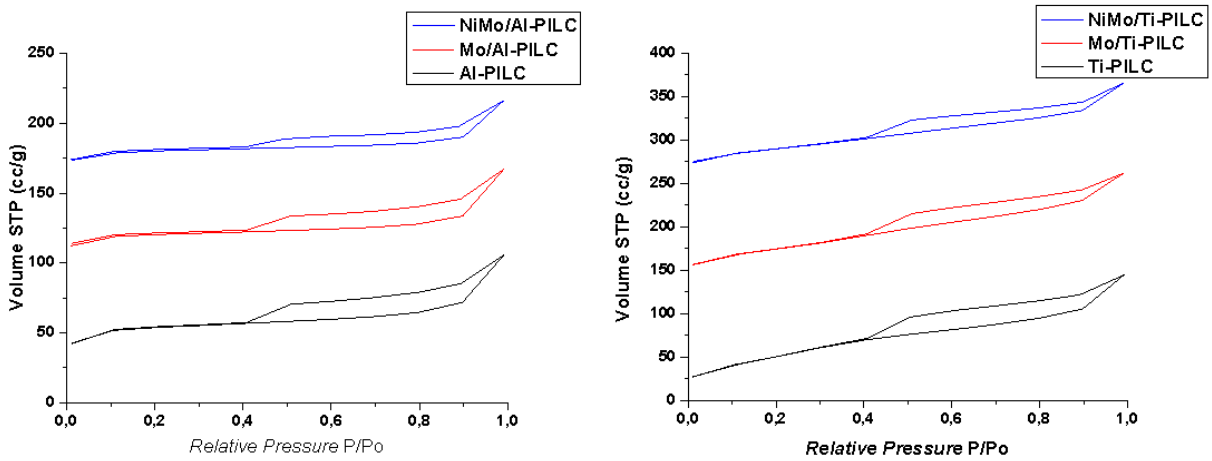


**Fig 2**. Adsorption-desorption isotherm graph of the prepared catalyst.

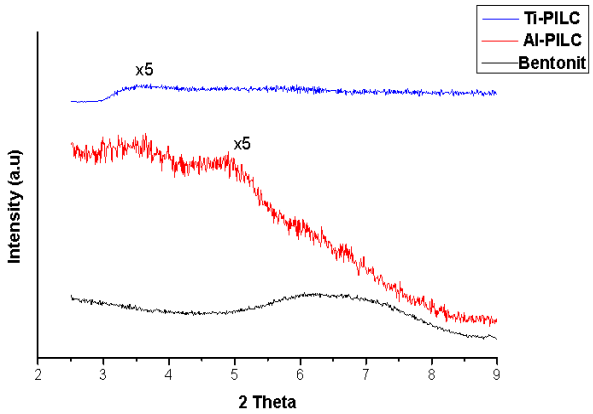


**Fig 3**. Low angel diffraction of bentonite, Al-PILC, and Ti-PILC.

increase in the basal space distance of interlayers bentonite; in other words, the preparation process using the pillarization method was successful (Haerudin *et al.*, 2010; Rinaldi *et al.*, 2023; Widjaya, 2012).

The results of wide-angle XRD analysis for Al-PILC, Mo/Al-PILC, and NiMo/Al-PILC catalyst samples are presented in Figure 4. The XRD analysis of bentonite revealed characteristic peaks at 2θ values of 19.70°, 26.61°, 35.31°, 54.45°, and 61.69°. Based on JCPDS No 29-1499, the Montmorillonite minerals possess the capacity for ion exchange and can alter pore structure (Widjaya, 2012). The pillarization process of bentonite with aluminum (Al) and titanium (Ti) metals did not change the montmorillonite structure, as evidenced by the persistence of characteristic montmorillonite peaks (Furimsky, 2000).

A decrease in intensity observed in the X-ray diffraction pattern (Fig. 4), although not significantly pronounced, particularly at around 2θ of 20° and 54°, attributed to the interaction between alumina and the crystal lattice of bentonite. This interaction leads to the integration of alumina into the crystal lattice of bentonite (Widjaya, 2012). After the Al-PILC catalyst is impregnated with Mo metal (Mo/Al-PILC), new peaks are observed in Fig. 4 at around 2θ angles of 12.8° and 23.5°. According to JCPDS No 5-0506, the characteristic peaks of $MoO_3$ are located at 2θ of 23.3°, and the research conducted by Zhu *et al.* (2013) mentions that the distinct peaks of $MoO_3$ appear at 2θ of 12.8°. Therefore, the appearance of peaks at 2θ angles of 23.5° and 12.8° indicates the presence of $MoO_3$ oxide (Zhu *et al.*, 2013). The emergence of these characteristic $MoO_3$ peaks can be attributed to the high concentration of added Mo metal (13 %wt) and its uneven dispersion on the surface of bentonite (Okamoto *et al.*, 1998). The appearance of $MoO_3$ oxide peaks makes it challenging to form active phases after the catalyst undergoes sulfidation (Ulfah & Subagjo, 2012). Based on JCPDS No 5-0506, the characteristic peaks of NiO oxide are located at 2θ angles of 43.46° and 63.11° (Rinaldi *et al.*, 2017). These NiO peaks were not detected in the NiMo/Al-PILC catalyst (Fig. 4), indicating that the added NiO oxide was well-dispersed and even on the surface of bentonite. Further support for the dispersion of Mo and Ni metals is observed in reducing the catalyst's surface area and pore volume (Table 1). The impregnation process with Mo and Ni metals does not change

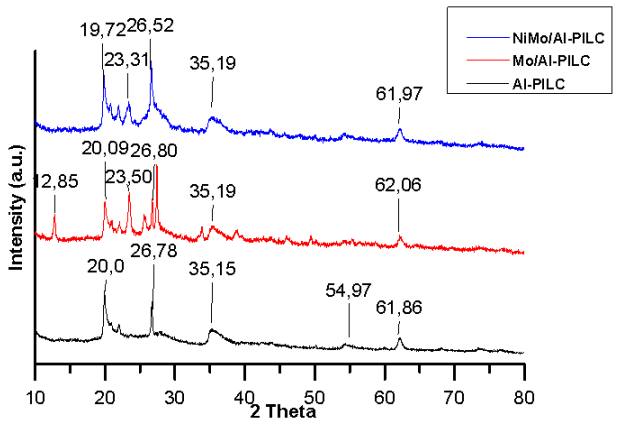


**Fig 4**. Wide angel diffraction of Al-PILC, Mo/Al-PILC, and NiMo/Al-PILC.

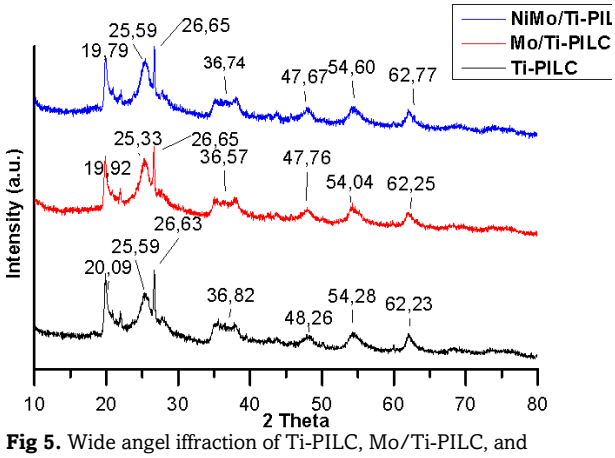


**Fig 5.** Wide angel iffraction of Ti-PILC, Mo/Ti-PILC, and NiMo/TI-PILC

**Table 2**
The acidity of the prepared catalysts by the $NH_3$-TPD analysis.

| Samples | Total Acidity (mmol/g) |
|---|---|
| Bentonite | 0.045 |
| Al-PILC | 0.134 |
| Mo/Al-PILC | 0.152 |
| NiMo/Al-PILC | 0.169 |
| Ti-PILC | 0.115 |
| Mo/Ti-PILC | 0.211 |
| NiMo/Ti-PILC | 0.178 |

the structure of bentonite since the characteristic peaks of bentonite remain visible in the X-ray diffraction pattern (Figure 4).

Results of the wide-angle analysis for Ti-PILC, Mo/Ti-PILC, and NiMo/Ti-PILC catalysts are presented in Fig. 5. Characterizing the titania-pillared catalyst aims to identify the constituent structure of titania, which typically consists of a mixture of anatase and rutile. The characterization results can be observed in Fig. 5, indicating that the peaks from the anatase crystal structure are more dominant than those from the rutile structure. The peak pattern of the anatase crystal structure aligns with the JCPDS No 71-1167 standard, as evidenced by the presence of high-intensity peaks at 2θ angles of 25.3° with Miller index (101), along with three other dominant peaks at 2θ angles of 38.6°, 48.1°, and 53.9° with respective Miller indices (004), (200), and (211). The characterization results for the prepared catalyst reveal characteristic peaks of $TiO_2$ anatase (Fig. 5). The $TiO_2$ anatase phase possesses a larger surface area than the rutile phase, thus potentially enhancing the catalyst's activity (Sumarlan *et al.*, 2017). The impregnation process of Mo and Ni metals into the catalyst forms $MoO_3$ and NiO oxides. The characterization results in Fig. 5 do not display characteristic peaks of Mo and Ni metals, indicating that these metals have been well-dispersed uniformly on the bentonite surface. Further support for the proper dispersion of Mo and Ni metals is evident in reducing the catalyst's surface area and pore volume (Table 1). The impregnation process with Mo and Ni metals does not change the structure of bentonite, as demonstrated in Fig. 5, where characteristic peaks of bentonite are still present.

The analysis of acid-strength catalysts through chemisorption is conducted using the Temperature Programmed Desorption-NH3 ($NH_3$-TPD) instrument to measure the amount of $NH_3$ gas adsorbed and desorbed by the catalyst. The quantity of $NH_3$ gas absorbed is directly proportional to the acidity strength of the catalyst (Peng *et al.*, 2014). The results of the $NH_3$-TPD analysis for the prepared catalysts are presented in Table 2.

Table 2 shows that the total acidity of Al-PILC and Ti-PILC is higher than that of bentonite, attributed to the fact that the cation exchange process in interlayer bentonite with Al and Ti pillar metals occurred successfully, thus elevating the acidity strength of the bentonite supported by Al and Ti metals. It is facilitated by the higher oxidation state and charge of Al and Ti metals, enabling them to exchange with buffering cations (Widjaya, 2012). Additionally, this is due to the silanol layer structure, where the oxide of the supporting metal is fully exchanged with Al and Ti ions. Al and Ti ions on the support are combined through Al-Si-OH group bonding to form medium to strong acid sites (Parangi & Mishra, 2020). Furthermore, this study demonstrates that the pillaring of Al and Ti on bentonite can significantly enhance the modified bentonite's acidity (Salerno *et al.*, 2004).

Impregnation of Mo metal into Mo/Al-PILC and Mo/Ti-PILC catalysts enhances their acid strength due to the relatively uniform distribution of Mo on the bentonite surface. This effect is attributed to partially filled d orbitals in Mo metal, facilitating the acceptance of free electron pairs from $NH_3$ (Ishii & Kyotani, 2016; Smart *et al.*, 2005). The acidity levels of Al-PILC and Ti-PILC increase after impregnation with Mo metal, with a significant increase observed in the case of Mo/Ti-PILC (Table 2). It is supported by XRD data (Figure 5), which shows the absence of characteristic peaks of $MoO_3$, indicating that Mo metal is evenly dispersed on the bentonite surface, thus enhancing acidity. Impregnating Ni metal into the catalyst also increases its acid strength, similar to Mo. The analysis results (Table 2) show that Mo/Al-PILC impregnated with Ni to become NiMo/Al-PILC experiences an increase in acidity, although not significantly.

In contrast, Mo/Ti-PILC slightly decreases acid strength after adding Ni to form NiMo/Ti-PILC. It might be due to Ni metal covering the acidic sites of the catalyst (Kou, 2000). Other data supporting the well-dispersed Mo and Ni metals resulting in increased acid strength include a decrease in specific surface area (Table 1). Catalysts with Ti-based pillars have a higher total acidity than Al-based ones because the positive charge of $Ti^{4+}$ ions is greater than that of $Al^{3+}$ ions (Binitha & Sugunan, 2006).

X-ray fluorescence (XRF) characterization aims to identify the content and composition of oxides formed during the pillarization and the impregnation process on bentonite. The XRF analysis results for the prepared catalysts are shown in Table 3.

From the oxide composition in bentonite, it obtained that Ca-montmorillonite is a type of bentonite used in this study (similar observed in the XRD result in Fig. 4). The amount of Al and Ti oxides increase after the pillarization process, followed by a decreased amount in the elemental of initial bentonite (Al, Si, and Ca). It is described that cation exchange proceeds in the interlayer bentonite during the pillarization. The value displayed by the instrument does not directly indicate the metal oxide content in the catalyst samples because the standard sample used is a mixture of several elements. Thus lower sensitivity and accuracy during the XRF analysis. Instead, they indicate qualitative data and the progress of the impregnation process (Rinaldi *et al.*, 2017).

Oxide $MoO_3$ was added at 13 wt% into Al-PILC and Ti-PILC to prepare Mo/Al-PILC and Mo/Ti-PILC, respectively. The results showed that the percentage of successfully impregnated $MoO_3$ oxide was 9.26% and 10.92%, confirming the effective

**Table 3**
The results of XRF measurement for the prepared catalysts.

| Samples | $Al_2O_3$(%) | $SiO_2$ (%) | $TiO_2$(%) | Ca) (%) | NiO(%) | $MoO_3$(%) |
|---|---|---|---|---|---|---|
| Bentonite | 20.01 | 61.89 | 0.2 | 1.58 | 0 | 0 |
| Al-PILC | 25.52 | 54.19 | 0.2 | 0.19 | 0 | 0 |
| Mo/Al-PILC | 21.69 | 47.48 | 0.16 | 0.18 | 0 | 9.26 |
| NiMo/Al-PILC | 19.78 | 47.01 | 0.20 | 10.19 | 5.07 | 14.56 |
| Ti-PILC | 12.36 | 42.29 | 31.41 | 0.33 | 0.01 | 0.02 |
| Mo/Ti-PILC | 10.91 | 38.35 | 21.35 | 0.29 | 0.01 | 10.92 |
| NiMo/Ti-PILC | 8.74 | 35.31 | 25.36 | 0.28 | 4.54 | 14.21 |

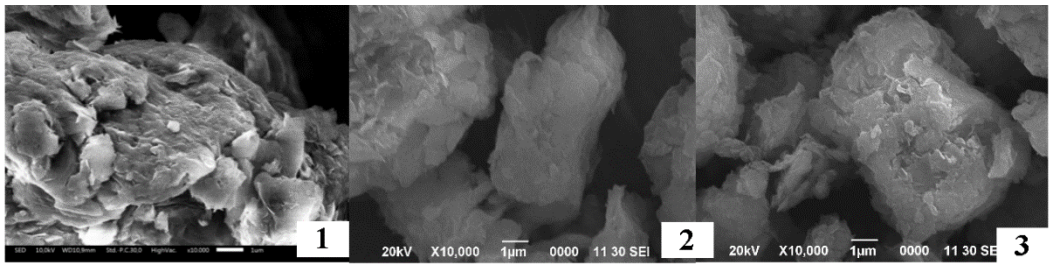


**Fig 6**. SEM results of the bentonite (1), Al-PILC (2), and Ti-PILC (3).

impregnation of Mo metal into the catalysts. On the other hand, NiO oxide was impregnated at 4 wt% into Mo/Al-PILC and Mo/Ti-PILC to prepare NiMo/Al-PILC and NiMo/Ti-PILC. The results indicated that the percentage of successfully impregnated Ni metal was 5.07% and 4.54%, respectively, signifying the successful impregnation of Ni metal into the catalysts. It aligns with the research conducted by Rinaldi *et al.* (2017), which showed that metals Mo and Ni were impregnated into bentonite mainly to detect the resulting NiO and $MoO_3$ oxides (Rinaldi *et al.*, 2017).

SEM characterization serves the purpose of identifying surface morphology and the distribution of components in the prepared catalyst. The SEM characterization results are presented in Figure 6. SEM analysis results in Fig. 6 reveal the morphology of bentonite, Al-PILC, and Ti-PILC. Bentonite exhibits a structure composed of soft layers that form bulky aggregates or particles. A similar morphology is observed for Al-PILC and Ti-PILC, which also appear to have soft alumina-silicate layers. However, based on Fig. 6 with the same magnification, it is evident that the aggregate size in Ti-PILC is smaller than Al-PILC's. Ti-PILC still shows a distribution of small aggregates, resulting in a much larger pore volume. It is supported by the pore volume and pore size data in Table 1.

Furthermore, Al-PILC and Ti-PILC catalysts have smoother surfaces and larger voids than bentonite. It is attributed to the impregnation with $Al_2O_3$ and $TiO_2$ oxides incorporated into bentonite. As a result, the specific surface area of Al-PILC and Ti-PILC catalysts increases (Table 1). Additionally, bentonite exhibits a denser structure compared to the morphology of Al-PILC and Ti-PILC.

Further SEM analysis results for the NiMo-prepared catalyst are described in Figure 7. SEM analysis results in Fig. 7 demonstrate that, generally, the surface morphology of NiMo/Al-PILC and NiMo/Ti-PILC catalysts consists of soft layers. After the impregnation of Mo and Ni onto the Al-PILC and Ti-PILC supports, it is evident that these metals are distributed relatively evenly on the support surfaces, as indicated by the absence of spots with varying color intensities (Susanto *et al.*, 2017). Furthermore, in the case of Mo/Al-PILC, it is observed that the aggregate size is more significant compared to Mo/Ti-PILC at the same magnification. This observation is also supported by the results in Table 1, which show that the specific surface area of Mo/Al-PILC is smaller than that of Mo/Ti-PILC. The addition of Ni metal results in a reduction in the aggregate size for both Mo/Al-PILC and Mo/Ti-PILC. This phenomenon can be attributed to the redispersion of Mo metal on the support's surface during the second impregnation step when Ni metal is added. These findings align with previous research conducted by Rinaldi (2017), which suggests that after the addition of Ni metal, there is a redistribution and redispersion of Mo metal on the support's surface (Kabe, T., Ishihara, A., Qian, 1999; Rinaldi *et al.*, 2017; Topsøe, H.; Clausen, B.S.; Massoth, 1996). These SEM characterization results also provide support for the XRD characterization data (Figs. 4 and 5), particularly in the case of Mo/Al-PILC, where a decrease in XRD intensity from $MoO_3$ diffraction is observed after the addition of Ni metal during the second impregnation step (Rinaldi *et al.*, 2017).

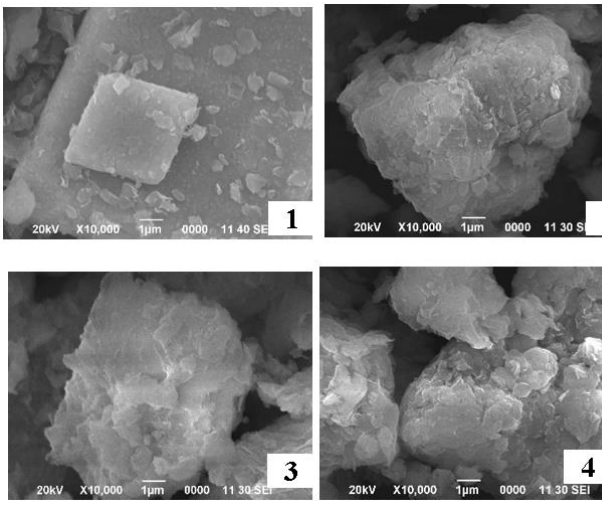


**Fig 7**. SEM results of Mo/Al-PILC (1) Mo/Ti-PILC(2) NiMo/AL-PILC (3), and NiMo/Ti-PILC (4).

### *3.2 Catalytic performance result*

The hydrodeoxygenation (HDO) reaction of guaiacol was carried out in a 100 mL autoclave reactor at a temperature of 573 K and a pressure of 60 bar ($H_2$ gas) for 2 hours. Before the reaction, all of the prepared catalysts undergo a sulfidation process, which involves the addition of sulfur to activate the catalyst (Kabe, T., Ishihara, A., Qian, 1999; Topsøe, H.; Clausen, B.S.; Massoth, 1996). The addition of $H_2S$ also serves to increase the acidity of the catalyst, facilitating the HDO reaction of guaiacol (Mora-Vergara *et al.*, 2018). Determining parameters such as temperature, pressure, and reaction time in the HDO of guaiacol followed the method used in the study by Liu K (2016). Decane was the solvent because guaiacol's HDO reaction products are nonpolar organic compounds. Therefore, the products produced would dissolve completely in decane. Isooctane was added as an internal standard on the liquid product to maintain the samples' measurement consistency using GC-FID (Liu, 2016).

The target compounds studied in this research are benzene, Phenol, and cyclohexane. Generally, these three compounds are selected because they are liquid products of the catalytic guaiacol hydrodeoxygenation (HDO) reaction (Mora-Vergara *et al.*, 2018). Benzene is one of the target compounds representing compounds that do not contain oxygen atoms but still have double bonds. Phenol serves as a representation of compounds containing oxygen atoms and double bonds. Cyclohexane is selected to represent compounds that do not contain oxygen atoms and double bonds. This study proposes a simple reaction scheme of the guaiacol HDO reaction just via the HDO pathway,

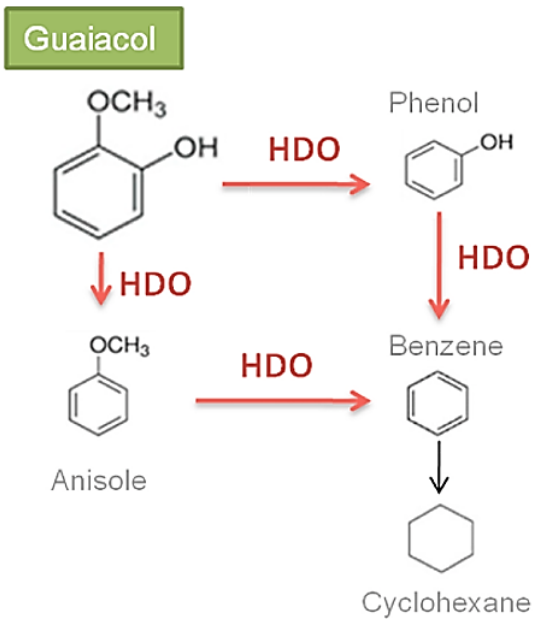


**Fig 8**. A Simple scheme of the HDO reaction of guaiacol via the HDO pathway.

as described in Figure 8. The scheme was inspired by studies conducted by Mora-Vergara *et al.* (2018)and Rivoira *et al.* (2021). With the HDO pathway (Fig.8), guaiacol is desired to convert to Phenol and anisole. After a consecutive HDO reaction, both products can be transformed into benzene, forming cyclohexane by the hydrogenation reaction (Mora-Vergara *et al.*, 2018; Rivoira *et al.*, 2021).

The performance of the prepared catalyst is evaluated based on the percentage of conversion and yield of the analyzed target compounds (Annisa, 2012). Percent conversion is calculated from the concentration difference of guaiacol before and after the reaction. The percent yield is measured by the concentration of the target compound formed divided by the concentration of guaiacol reacted. Table 4 shows the activity results of the prepared catalysts on the HDO guaiacol reaction with a pressure of 60 bar, temperature of 573 K, and reaction time of 2 hours.

Using bentonite as a catalyst shows that it is inactive in the HDO guaiacol reaction (Table 4). No benzene, phenol, or cyclohexane compounds were detected, and the guaiacol concentration almost did not change after the reaction. It is suggested because the acidity level of bentonite is trim; thus, the small number of $H^+$ ions makes breaking the bonds between OH or methyl with the benzene ring difficult (Parangi & Mishra, 2020). It is supported by the results of the $NH_3$-TPD analysis (Table 2), which showed that bentonite had a minimal acidity of 0.045 mmol/gram. Furthermore, the specific surface area of bentonite is also exceedingly low, as shown by the BET analysis in Table 1, further constraining its activity. Adding Al and Ti pillar metals, combined with active metals Ni and Mo impregnated onto the catalyst, will provide empty d orbitals or unpaired electrons interacting with guaiacol (as the reactant). This interaction forms new bonds with specific strengths or energies that can facilitate the conversion of guaiacol into its respective products (Campbell, 1988).

Table 4 clearly shows that the catalytic activity of bentonite < Mo/Al-PILC < Mo/Ti-PILC < Al-PILC = Ti-PILC < NiMo/Al-PILC < NiMo/Ti-PILC based on percent conversion calculations. The superior conversion of the NiMo/Ti-PILC catalyst compared to other catalysts is suggested because the main factor is the well dispersion of the active metals Mo and Ni on the surface or in the pores of the support, followed by the factors of surface area, pore volume, pore size, and acidity.

The results of $N_2$ gas adsorption (Table 1) and $NH_3$-TPD analysis (Table 2) show that although the surface area and pore volume of the NiMo/Ti-PILC catalyst is smaller than the Al-PILC and Ti-PILC catalysts, the acidity value of NiMo/Ti-PILC is more remarkable than both, Al-PILC and Ti-PILC. Thus, the HDO guaiacol reaction conversion of the NiMo/Ti-PILC catalyst is higher than the Al-PILC and Ti-PILC catalysts. The higher acidity value of the catalyst illustrates the large number of donors ion $H^+$ it has, therefore the greater its ability to split OH bonds and methyl oxygen bonds with the aromatic ring (Parangi & Mishra, 2020).

Considering the conversion of guaiacol via the HDO reaction pathway, an active metal catalyst needs to be dispersed on the surface of the support. Thus, it can capture $H^+$ ions from $H_2$ gas and directly react to convert the guaiacol raw material. However, the dispersion of active metal onto the surface support causes a decrease in surface area and pore volume. Therefore, the Mo/Al-PILC and Mo/Ti-PILC catalysts have less reaction conversion than the Al-PILC and Ti-PILC supports. It is concluded that the surface area and pore volume are the main significant factors influencing the HDO guaiacol reaction compared with the acidity value.

The Ni metal addition as a promoter to the Mo/Al-PIC and Mo/Ti-PILC catalysts caused a significant increase in the conversion of the HDO guaiacol reaction (Table 4). It is because of an increase in the catalyst's ability in hydrogenolysis performance, especially on the methyl - oxygen bond and the OH bond with the aromatic ring so that guaiacol is more easily converted into the desired target product (Kabe, T., Ishihara, A., Qian, 1999; Mora-Vergara *et al.*, 2018; Topsøe, H.; Clausen, B.S.; Massoth, 1996). Therefore, the conversion of HDO guaiacol reaction significantly increased on NiMo/Al-PILC and NiMo/Ti-PILC catalysts after adding Ni promoter metal. Table 4 also observes that the NiMo/Ti-PILC catalyst has a higher guaiacol conversion than the NiMo/Al-PILC catalyst. XRD analysis data (Fig. 2) obtain a well dispersion of Mo and Ni

**Table 4**
The performance results of the prepared catalysts on the HDO reaction of Guaiacol.

| Samples | Guaiacol Conv. (%) | Yield of Fenol (%) | Yield of Cyclohexane (%) | Yield of Benzene (%) |
|---|---|---|---|---|
| Bentonite | - | - | - | - |
| Al-PILC | 47 | 58 | - | - |
| Mo/Al-PILC | 33 | 74 | - | - |
| NiMo/Al-PILC | 52 | 42 | 0.5 | - |
| Ti-PILC | 46 | 54 | 0.1 | - |
| Mo/Ti-PILC | 36 | 86 | 0.7 | - |
| NiMo/Ti-PILC | 70 | 50 | 0.4 | 0.08 |

**Table 5**
Percent conversion results of the HDO guaiacol reaction with the temperature and time variations.

| Temperature (K) | Time (h) | Conversion (%) |
|---|---|---|
| | 2 | 7.28 |
| 523 | 3 | 27.62 |
| | 4 | 39.89 |
| | 2 | 69.80 |
| 573 | 3 | 80.94 |
| | 4 | 99.46 |
| | 2 | 99.26 |
| 623 | 3 | 98.26 |
| | 4 | 99.91 |

metals on the surface support, especially the Ti-PILC support. It will produce a lot of active sites of the catalyst after the sulfidation. Thus, the guaiacol conversion will be the highest compared to other catalysts, especially the NiMo/Al-PILC catalyst. Furthermore, besides the extensive conversion of guaiacol due to its high HDO reaction activity, the NiMo/Ti-PILC catalyst is also very active for the hydrodeoxygenation (HYD) reaction, as shown in Table 4 that only the NiMo/Ti-PILC catalyst which obtains the highest percent yield of the benzene product (Adilina *et al.*, 2019; Liu, 2016; Romero *et al.*, 2010).

### *3.3 Effect of temperature and reaction time on the HDO Guaiacol*

Time and temperature variations were carried out in the HDO guaiacol reaction using a NiMo/Ti-PILC catalyst. Besides finding optimum reaction conditions, studying the effects of temperature and reaction time on the HDO guaiacol reaction is essential. The NiMo/Ti-PILC catalyst is used at this stage because it has the highest percent conversion value, namely 70%, compared to other catalysts. The result analysis of percent conversion over time and temperature variations on the NiMo/Ti-PILC catalyst for the HDO guaiacol reaction is presented in detail in Table 5.

According to Liu K (2016), the percentage conversion is influenced by various parameters, including temperature and time, where an increase in temperature and reaction time correlates linearly with the resulting percentage conversion (Liu, 2016). The test results indicate that the percentage conversion obtained increases as the temperature and reaction time during guaiacol HDO increase. This aligns with the research by Liu K (2016), which suggests that higher temperatures and longer reaction times are directly proportional to the resulting percentage conversion. These findings are consistent with the results of the study conducted by Guierrez (2009), which demonstrated similar outcomes. Elevated temperatures and duration reaction times can lead to rapid movement of the reactant (guaiacol), resulting in more frequent contact with the catalyst, consequently leading to a higher production of products or an increased percentage conversion (Gutierrez *et al.*, 2009; Huang *et al.*, 2013; Lee *et al.*, 2012; Rivoira *et al.*, 2021). The highest percent conversion is obtained with a temperature reaction of 623 K for four hours (Tabel 5).

## 4. Conclusion

The pillarization process of bentonite using Al and Ti metals as the pillaring agent has been prepared successfully. The XRD analysis observed a shift in the small angle 2θ ($d_{001}$) of bentonite after the pillarization process. Likewise, the preparation of the NiMo supported by pillared bentonite Al and Ti catalyst was also successfully obtained via the stepwise impregnation method. Several characterization results showed increased physicochemical properties compared to raw bentonite or even bentonite pillared. The sulfide NiMo/Ti-PILC catalyst performed the highest conversion of 70% on the HDO reaction of guaiacol. At various conditions of reaction time and temperature during the HDO reaction of guaiacol, the higher reaction temperatures and longer reaction times resulted in higher conversion.

## Acknowledgments

The authors would like to express their gratitude for the funding from the Deputy of Sciences and Technology, Indonesian Institute of Sciences. Also, thank Mr. Hendris Hendarsyah Kurniawan for supporting and fruitful discussion of the analysis of catalyst test results in the HDO guaiacol reaction.

**Author Contributions**: NR, NLS, S: Conception and design of study; NR, NLS, S, AAD: Acquisition of data; NR, NLS, EA, RRW, AAD: Analysis and/or interpretation of data; NR, NLS, S: Drafting the manuscript; NR, NLS, EA, RRW, AAD: Revising the manuscript critically for important intellectual content; All authors (NR, NLS, S, EA, RRW, AAD): Approval of the version of the manuscript to be published

**Funding:** This research was funded by the internal institution (Indonesian Institute of Sciences). The author(s) received no financial support for the authorship, and/or publication of this article.

**Conflicts of Interest:** The authors declare that they have no known competing financial interests or personal relationships that could have appeared to influence the work reported in this work.

## References

Adams, P., Bridgwater, T., Lea-Langton, A., Ross, A., & Watson, I. (2018). Biomass Conversion Technologies. In *Greenhouse Gases Balances of Bioenergy Systems* (pp. 107–139). Elsevier. https://doi.org/10.1016/B978-0-08-101036-5.00008-2

Adilina, I. B., Rinaldi, N., Simanungkalit, S. P., Aulia, F., Oemry, F., Stenning, G. B. G., Silverwood, I. P., & Parker, S. F. (2019). Hydrodeoxygenation of Guaiacol as a Bio-Oil Model Compound over Pillared Clay-Supported Nickel–Molybdenum Catalysts. *The Journal of Physical Chemistry C*, *123*(35), 21429–21439. https://doi.org/10.1021/acs.jpcc.9b01890

Amaya, J., Bobadilla, L., Azancot, L., Centeno, M., Moreno, S., & Molina, R. (2020). Potentialization of bentonite properties as support in acid catalysts. *Materials Research Bulletin*, *123*, 110728. https://doi.org/10.1016/j.materresbull.2019.110728

Annisa, G. (2012). *Hydrodeoxygenation of bio-oilUsing CoMo/C catalyst for optimizing alkane dan alcohol production* [Thesis, Universitas Indonesia]. https://lib.ui.ac.id/detail?id=20313952

Binitha, N. N., & Sugunan, S. (2006). Preparation, characterization and catalytic activity of titania pillared montmorillonite clays. *Microporous and Mesoporous Materials*, *93*(1–3), 82–89. https://doi.org/10.1016/j.micromeso.2006.02.005

Bu, Q., Lei, H., Zacher, A. H., Wang, L., Ren, S., Liang, J., Wei, Y., Liu, Y., Tang, J., Zhang, Q., & Ruan, R. (2012). A review of catalytic hydrodeoxygenation of lignin-derived phenols from biomass pyrolysis. *Bioresource Technology*, *124*, 470–477. https://doi.org/10.1016/j.biortech.2012.08.089

Campbell, I. M. (1988). *Catalysis at Surfaces* (First Edit). Chapman and

Hall.
de Miguel Mercader, F., Groeneveld, M. J., Kersten, S. R. A., Geantet, C., Toussaint, G., Way, N. W. J., Schaverien, C. J., & Hogendoorn, K. J. A. (2011). Hydrodeoxygenation of pyrolysis oil fractions: process understanding and quality assessment through co-processing in refinery units. *Energy & Environmental Science*, *4*(3), 985. https://doi.org/10.1039/c0ee00523a
Furimsky, E. (2000). Catalytic hydrodeoxygenation. *Applied Catalysis A: General*, *199*(2), 147–190. https://doi.org/10.1016/S0926-860X(99)00555-4
Gutierrez, A., Kaila, R. K., Honkela, M. L., Slioor, R., & Krause, A. O. I. (2009). Hydrodeoxygenation of guaiacol on noble metal catalysts. *Catalysis Today*, *147*(3–4), 239–246. https://doi.org/10.1016/j.cattod.2008.10.037
Haerudin, H., Rinaldi, N., & Fisli, A. (2010). Characterizatio of modified bentonite using aluminium polycation. *Indonesian Journal of Chemistry*, *2*(3), 173–176. https://doi.org/10.22146/ijc.21913
Huang, J., Li, X., Wu, D., Tong, H., & Li, W. (2013). Theoretical studies on pyrolysis mechanism of guaiacol as lignin model compound. *Journal of Renewable and Sustainable Energy*, *5*(4). https://doi.org/10.1063/1.4816497
Ishii, T., & Kyotani, T. (2016). Temperature Programmed Desorption. In *Materials Science and Engineering of Carbon* (pp. 287–305). Elsevier. https://doi.org/10.1016/B978-0-12-805256-3.00014-3
Kabe, T., Ishihara, A., Qian, W. (1999). *Hydrodesulfurization and Hydrodenitrogenation*. Kodansha and Wiley-VCH.
Kar, Y. (2018). Catalytic cracking of pyrolytic oil by using bentonite clay for green liquid hydrocarbon fuels production. *Biomass and Bioenergy*, *119*, 473–479. https://doi.org/10.1016/j.biombioe.2018.10.014
Khairina, N. N. L., Kristiani, A., Widjaya, R. R., Agustian, E., Dwiatmoko, A. A., & Rinaldi, N. (2022). Conversion of fatty acid into biodiesel using solid catalysts of Ti-Zr and Ti-Cr pillared bentonite. *AIP Conference Proceedings*, 2493(1), 060017. https://doi.org/10.1063/5.0110942
Kou, M. R. S. (2000). Evaluation of the Acidity of Pillared Montmorillonites by Pyridine Adsorption. *Clays and Clay Minerals*, *48*(5), 528–536. https://doi.org/10.1346/CCMN.2000.0480505
Kubička, D., & Kaluža, L. (2010). Deoxygenation of vegetable oils over sulfided Ni, Mo and NiMo catalysts. *Applied Catalysis A: General*, *372*(2), 199–208. https://doi.org/10.1016/j.apcata.2009.10.034
Lee, C. R., Yoon, J. S., Suh, Y.-W., Choi, J.-W., Ha, J.-M., Suh, D. J., & Park, Y.-K. (2012). Catalytic roles of metals and supports on hydrodeoxygenation of lignin monomer guaiacol. *Catalysis Communications*, *17*, 54–58. https://doi.org/10.1016/j.catcom.2011.10.011
Liu, K. (2016). *Catalytic hydrodeoxygenation of bio-oil and model compounds* [Imperial College London]. http://hdl.handle.net/10044/1/51555
Mohan, D., Pittman, C. U., & Steele, P. H. (2006). Pyrolysis of Wood/Biomass for Bio-oil: A Critical Review. *Energy & Fuels*, *20*(3), 848–889. https://doi.org/10.1021/ef0502397
Mora-Vergara, I. D., Hernández Moscoso, L., Gaigneaux, E. M., Giraldo, S. A., & Baldovino-Medrano, V. G. (2018). Hydrodeoxygenation of guaiacol using NiMo and CoMo catalysts supported on alumina modified with potassium. *Catalysis Today*, *302*, 125–135. https://doi.org/10.1016/j.cattod.2017.07.015
Mortensen, P. M., Grunwaldt, J.-D., Jensen, P. A., Knudsen, K. G., & Jensen, A. D. (2011). A review of catalytic upgrading of bio-oil to engine fuels. *Applied Catalysis A: General*, *407*(1–2), 1–19. https://doi.org/10.1016/j.apcata.2011.08.046
Niemantsverdriet, J. W. (2007). *Spectroscopy in Catalysis*. Wiley. https://doi.org/10.1002/9783527611348
Nugrahaningtyas, K. D., Hidayat, Y., & Prayekti, P. S. (2015). Aktivitas dan selektivitas katalis Mo-Co/USY pada reaksi hidrodeoksigenasi anisol. *Jurnal Penelitian Saintek*, *20*(1). https://doi.org/10.21831/jps.v20i1.5609
Okamoto, Y., Umeno, S., Arima, Y., Nakai, K., Takahashi, T., Uchikawa, K., Inamura, K., Akai, Y., Chiyoda, O., Katada, N., Shishido, T., Hideshi Hattori, Hasegawa, S., Yoshida, H., Segawa, K., Koizumi, N., Yamada, M., Nishijima, A., Kabe, T., … Uchijima, T. (1998). A study on the preparation of supported metal oxide catalysts using JRC-reference catalysts. I. Preparation of a molybdena–alumina catalyst. Part 3. Drying process. *Applied Catalysis A: General*, *170*(2), 343–357. https://doi.org/10.1016/S0926-860X(98)00066-0
Parangi, T., & Mishra, M. K. (2020). Solid Acid Catalysts for Biodiesel Production. *Comments on Inorganic Chemistry*, *40*(4), 176–216. https://doi.org/10.1080/02603594.2020.1755273
Peng, S.-Y., Xu, Z.-N., Chen, Q.-S., Wang, Z.-Q., Chen, Y., Lv, D.-M., Lu, G., & Guo, G.-C. (2014). MgO: an excellent catalyst support for CO oxidative coupling to dimethyl oxalate. *Catal. Sci. Technol.*, *4*(7), 1925–1930. https://doi.org/10.1039/C4CY00245H
Rinaldi, N., Purba, N. D. E., Kristiani, A., Agustian, E., Widjaya, R. R., & Dwiatmoko, A. A. (2023). Bentonite pillarization using sonication in a solid acid catalyst preparation for the oleic acid esterification reaction. *Catalysis Communications*, *174*, 106598. https://doi.org/10.1016/j.catcom.2022.106598
Rinaldi, N., Simanungkalit, S. P., & Kristiani, A. (2017). Hydrodeoxygenation of bio-oil using different mesoporous supports of NiMo catalysts. *AIP Conference Proceedings*,1904(1),020078. https://doi.org/10.1063/1.5011935
Rivoira, L., Martínez, M. L., & Beltramone, A. (2021). Hydrodeoxygenation of guaiacol over Pt-Ga-mesoporous catalysts. *Microporous and Mesoporous Materials*, *312*, 110815. https://doi.org/10.1016/j.micromeso.2020.110815
Romero, Y., Richard, F., & Brunet, S. (2010). Hydrodeoxygenation of 2-ethylphenol as a model compound of bio-crude over sulfided Mo-based catalysts: Promoting effect and reaction mechanism. *Applied Catalysis B: Environmental*, *98*(3–4), 213–223. https://doi.org/10.1016/j.apcatb.2010.05.031
Salerno, P., Mendioroz, S., & López Agudo, A. (2004). Al-pillared montmorillonite-based NiMo catalysts for HDS and HDN of gas oil: influence of the method and order of Mo and Ni impregnation. *Applied Catalysis A: General*, *259*(1), 17–28. https://doi.org/10.1016/j.apcata.2003.09.019
Şenol, O. İ., Viljava, T.-R., & Krause, A. O. I. (2005). Hydrodeoxygenation of aliphatic esters on sulphided NiMo/γ-Al2O3 and CoMo/γ-Al2O3 catalyst: The effect of water. *Catalysis Today*, *106*(1–4), 186–189. https://doi.org/10.1016/j.cattod.2005.07.129
Sing, K. S. W. (1982). Reporting physisorption data for gas/solid systems with special reference to the determination of surface area and porosity (Provisional). *Pure and Applied Chemistry*, *54*(11), 2201–2218. https://doi.org/10.1351/pac198254112201
Smart, L. E., Moore, L. E., Smart, L. E., & Moore, E. A. (2005). *Solid State Chemistry*. CRC Press. https://doi.org/10.1201/b12396
Sumarlan, I., Fatimah, I., & Wijaya, K. (2017). Sintesis dan karakterisasi fotokatalis TiO2 Montmorilant terpilar alumina. *Jurnal Pijar Mipa*, *11*(2). https://doi.org/10.29303/jpm.v11i2.108
Susanto, B. H., Prakasa, M. B., & Shahab, M. H. (2017). Preparation and Characterization of NiMo/C Using Rapid Heating and Cooling Method for Renewable Diesel Synthesis from Nyamplung Oil (Calophyllum Inophyllum Oil). *INSIST*, *2*(1), 42. https://doi.org/10.23960/ins.v2i1.32
Thommes, M., Kaneko, K., Neimark, A. V., Olivier, J. P., Rodriguez-Reinoso, F., Rouquerol, J., & Sing, K. S. W. (2015). Physisorption of gases, with special reference to the evaluation of surface area and pore size distribution (IUPAC Technical Report). *Pure and Applied Chemistry*, *87*(9–10), 1051–1069. https://doi.org/10.1515/pac-2014-1117
Topsøe, H.; Clausen, B.S.; Massoth, F. E. (1996). *Hydrotreating Catalysis -Science and Technology* (Anderson,). Springer.
Ulfah, M., & Subagjo, S. (2012). Pengaruh perbedaan sifat penyangga alumina terhadap sifat katalis hydrotreating berbasis nikel-molibdenum. *Reaktor*, *14*(2), 151. https://doi.org/10.14710/reaktor.14.2.151-157
Widjaya, R. R. (2012). Bentonit Cr-Pillared and Zeolite HZSM-5 Catalysts For Conversion Process Ethanol to be Biogasoline [Universitas Indonesia]. https://lib.ui.ac.id/detail.jsp?id=20308024
Xu, Y., Wang, T., Ma, L., Zhang, Q., & Liang, W. (2010). Upgrading of the liquid fuel from fast pyrolysis of biomass over MoNi/γ-Al2O3 catalysts. *Applied Energy*, *87*(9), 2886–2891. https://doi.org/10.1016/j.apenergy.2009.10.028
Zhu, X., Cho, H., Pasupong, M., & Regalbuto, J. R. (2013). Charge-Enhanced Dry Impregnation: A Simple Way to Improve the

Preparation of Supported Metal Catalysts. *ACS Catalysis*, *3*(4), 625–630. https://doi.org/10.1021/cs3008347